Tacim *et al.*
International Journal of Geo-Engineering (2023) 14:6
https://doi.org/10.1186/s40703-023-00183-0

International Journal of Geo-Engineering

TECHNICAL NOTE

Open Access

Importance of grouting for tunneling in karstic and complex environment (a case study from Türkiye)

Gokhan Tacim[1], Evren Posluk[2] and Candan Gokceoglu[3*]

*Correspondence:
cgokce@hacettepe.edu.tr;
candan.gokceoglu@gmail.com

[1] TCDD, General Directorate of Turkish Railway System, Altindag, 06050 Ankara, Türkiye
[2] Institute of Graduate Studies, Istanbul University-Cerrahpaşa, Avcılar, 34320 Istanbul, Türkiye
[3] Department of Geological Engineering, Hacettepe University, Beytepe, 06800 Ankara, Türkiye

Abstract

In the planning of the tunnel support system, besides the detailed investigation of the geological-geotechnical conditions, it is also important to investigate the structure-tunnel interaction. Especially the structures located in the close vicinity of the tunnels built in unpredictable geological conditions should be considered as a part of the tunnel support system design and the planning should be performed. However, the strong heterogeneity and anisotropy characteristics of karstic environments affect the planning. In this study, a single-track railway tunnel excavated in a relatively thin-bedded, karstic limestone in the Gebze Köseköy Railway project is investigated in terms of structure-tunnel interaction and the importance of grouting. The fact that the tunnel, located in the center of the two piers of the Osmangazi Suspension Bridge approach viaducts, built on the Gulf of Izmit, passes through a shallow overburden, is also an important difficulty in the design of the tunnel. Some karstic caves are determined in the limestones besides its heavily fractured nature. It is concluded that there is a possibility of damage to the bridge as a result of different settlements under the viaduct piers during the tunnel construction with the support to be performed only through the tunnel, and the karstic caves should be filled in order to prevent possible damages. The karstic limestones along the tunnel route are strengthened from the surface by injection of a mixture of water, cement, bentonite, and sand. The interaction of the tunnel with the viaduct after injection is investigated with 2D and 3D numerical analysis and tunnel excavation and support works are started. With the tunnel construction, measurements taken from inside the tunnel and from the viaduct piers, values very close to the predicted deformation limits were obtained by 3D numerical analysis, and the tunnel construction is successfully completed. Despite the extremely difficult conditions, the main reason why no problems are encountered during the tunnel construction is considered to be the grouting.

Keywords: Tunnel, Karst, Grouting, Structure-tunnel interaction, 2D and 3D numerical analysis

Introduction

Shallow tunneling induces both lateral and vertical surface movements [14]. Ground settlement (surface vertical movement) is a critical threat to both the surface [43] and subsurface facilities [56]. Containing significant infrastructure in and around the proposed

tunnel location, the assumption of an undeveloped site may lead to a significant error in the predicted ground surface settlement [28]. Various studies have considered the case of tunnel construction interaction. It has been recognized that the building stiffness should be taken into account in the assessment of tunnel-structure interaction since it generally tends to decrease the structural distortions and risk of damage with respect to the greenfield case [20, 25–27, 29, 40]. On the other hand, the tunnel-single pile and pile group interaction problems have been widely analyzed using field trials, physical modeling, and numerical simulations, leading to some confidence in the assessment of pile group displacements [18, 19, 26, 34, 35, 41], internal forces [32, 37, 44, 53], and pile failure due to tunnel excavation [42]. However, a great majority of these cases are urban tunnels in weak ground conditions. Although ground conditions are good, there can be some serious engineering problems.

Some tunnel–structure interaction problems in karstic regions were reported (i.e. [3]. The design and construction of tunnels in karst terrains are extremely difficult due to the problems associated with the unexpected location, irregular geometry, and unpredictable dimensions of the karst structures [3]. Karst formations are characteristic of strong heterogeneity and anisotropy due to complex void structures, typically consisting of three levels of voids, i.e., primary porosity, secondary fractures, and tertiary conduits [9, 49]. The karst conduits, faults, and fractures provide the main channels for groundwater flow in karst formations, and the flow may deviate significantly from the laminar condition described by Darcy's law as the flow rate or hydraulic gradient increases [16, 17]. This unpredictable nature of karstic structures requires special research and approaches in tunnel design studies. Although filling the karstic caves is the first solution that comes to mind, the complexity of the filling type and construction methodologies should be solved. Chemicals and cement-based (mixtures such as water-cement, sand, bentonite, fly ash, etc.) are used as filling material. However, the most economical solution is still cement-based injections. As stated by [16, 17], due to poor geological conditions and unsymmetrical tunnel pressure, bridge stability is of great concern during tunneling. Consequently, depending on the increasing population, the need for underground rail transport is increasing in densely populated areas. Constructing tunnels in areas with dense settlements and various infrastructures is extremely difficult compared to virgin areas. Because there is a possibility that excessive deformations and/or failures that may occur during tunnel construction may also affect the structures in their close vicinity. However, relatively low deformations are expected when tunnel excavations are performed in good-quality rock masses. However, the presence of karstic caves whose dimensions cannot be estimated exactly can cause unexpected sudden failures.

Some parts of the shallow T5-1 tunnel were constructed in thin-bedded karstic dolomitic limestones. The T5-1 tunnel is located between the approaching viaducts of Osman Gazi Bridge. Osmangazi Bridge or Izmit Körfez Bridge is the fourth longest span suspension bridge in the World, with a middle span of 1550 m and a total length of 2682 m, built between Dilovası and Altınova in the Gulf of Izmit, Türkiye. The T5-1 tunnel, which is located in the middle of the Osman Gazi Bridge approach viaducts, is extremely critical with this feature. The presence of karstic caves and this special location constitute the main problems. Therefore, taking into account the possibility of serious effects of excessive deformations and/or failure on the Bridge that may occur during

the construction of the T5-1 tunnel, a certain part of which is located in the rocks with karstic features, it has become necessary to take precautions before excavations. Therefore, this study aims to evaluate the performance of the grouting performed before the excavation of the T5-1 tunnel, which was built in a karstic and complex environment. For this purpose, within the scope of the study, a case that is thought to be important in terms of tunneling literature is presented, considering the interaction of the T5-1 tunnel with the Osmangazi Bridge. In this context, the geomechanical properties of the geological unit were determined by interpreting the hydraulic properties and laboratory test data to put forward the bridge-tunnel interaction. Then, the situations before and after the injection of the karstic caves were investigated with the 3-Dimensional Finite Element analysis. The injection applied with a mixture of water, cement, and bentonite from the surface was evaluated by comparing the numerical results and in-situ measurements.

Project description

The majority of the population in Türkiye lives in a narrow region between Istanbul and Kocaeli provinces. The presence of intense industrial and port facilities in this region reveals the need for freight and passenger transportation. By increasing the capacity of the existing 2-line railway, which was built in 1873, 1 main and 1 connection railway line was designed next to the existing line to meet the need. The T5-1 Tunnel, which is the subject of this study, is located on the Gebze-Köseköy railway project route and has a length of 230 m (Km: 53 + 930 and 54 + 160). The northern approach viaducts (P-02 and P-03) of the Osman Gazi Bridge, located on the route of Gebze—Orhangazi İzmir Highway and built on the Gulf of Izmit, is located between the side piers (Figs. 1, 2).

The T5-1 Tunnel is designed as a single-track railway tunnel and is 7.45 m wide and 6.25 m high. It is planned to be excavated with the classical excavation method, New Austrian Tunneling Method (NATM), and has an excavation area of 64.32 m^2 (Fig. 2). The thickness of the overburden varies between 7 and 27 m When considering the location and geotechnical conditions, the T5-1 tunnel is a scientifically very interesting case

Fig. 1 Gebze-Köseköy project and T5-1 Tunnel location (Google Earth)

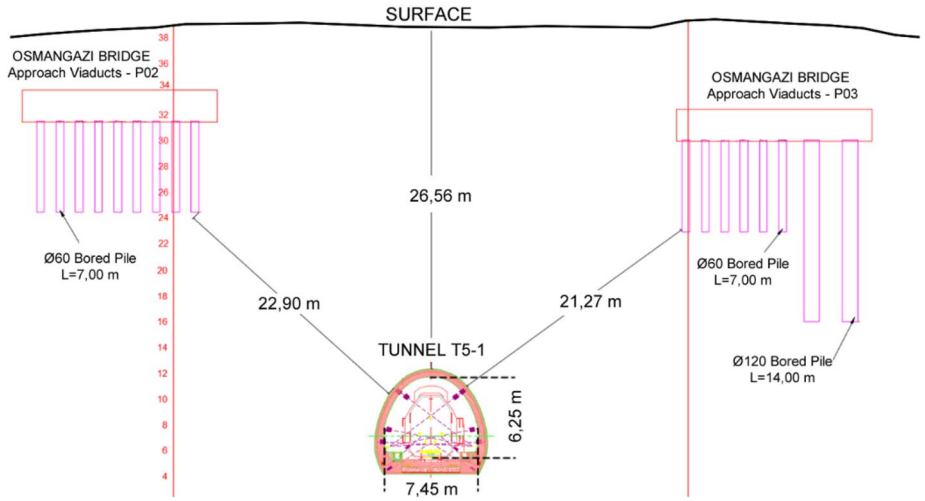

Fig. 2 Relationship between T5-1 Tunnel and Osmangazi Bridge north approach viaduct

for tunnel engineers. In addition, with the development of infrastructure, new tunnel crossings below existing bridges are becoming increasingly common [16, 17].

Geological and geotechnical settings

The tunnel route passes through thin-bedded, gray dolomitic limestone (Hereke Formation, [4] with interbedded Triassic marl (Figs. 3a, b). Karstification is frequently observed in the unit [24]. The unit has a moderate to slightly weathered structure in other places along the weak zones. The strength of the unit varies from weak to very solid.

When the foundations of Osman Gazi Bridge Approach Viaducts are examined, there is siltstone and mudstone interbedded brecciated limestone under the P-02 pier, while dolomitic limestone with clay intermediate level is found under the P-03 pier. These two unit boundaries are transitional with the shear zone (Fig. 3c). Although the shear zone is not encountered on the tunnel route, the presence of the shear zone is extremely important in terms of the interaction between the structure on the piles and the tunnel. The site locates in one of the most active seismic zones of Türkiye (Fig. 4).

In order to understand and examine the geological and geotechnical conditions of the tunnel route, in addition to the surface observations in the viaduct and tunnel area, the geological cross-section along the tunnel route was obtained by examining 7 drilling data (Fig. 5), and related tests were carried out in the laboratory and in-situ to determine the physicomechanical and elastic properties of the lithological units (Table 1).

Clay bands are observed in most of the tunnel overburden and the groundwater level is approximately 5.5 m below the tunnel base. During the drilling, karstic cavities were encountered 2.5 m below the tunnel base. The permeability of the bedrock forming the tunnel route was performed using the Lugeon test procedures recommended by Yihdego [57] in the drillings and evaluated with the Lugeon graphic method (Fig. 6).

At the exit portal of the tunnel, a highly permeable structure between 1 and 22 m from the surface, permeable between 22 and 37 m, and low permeable between 37 and 40 m was detected. When the drilling data and Lugeon values were evaluated together, it was understood that the rock conditions on the tunnel route included very fractured-cracked

Fig. 3 Geological units observed around the tunnel (**a**: dolomitic limestone, **b**: marl, **c**: boundary between limestone and marl, black line: layers, blue line: shear zone)

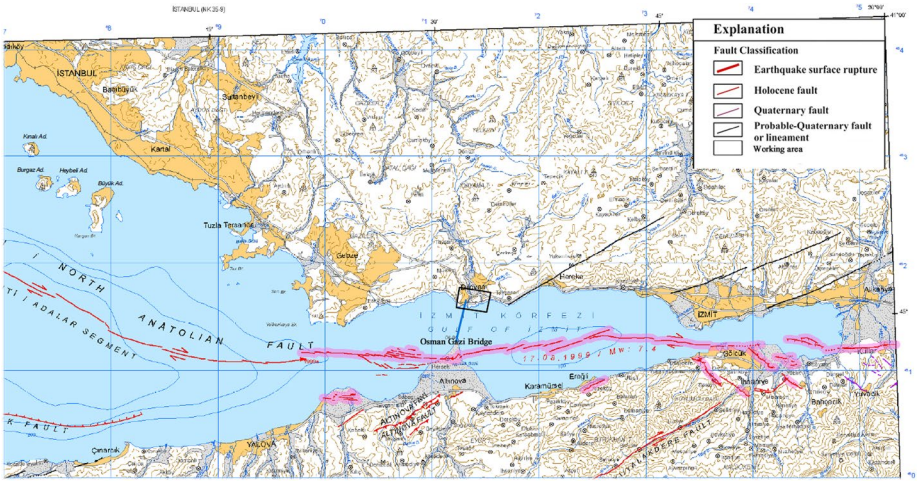

Fig. 4 Seismotectonic map of the Marmara Region of Türkiye [23]

and in places karstic cavities. During the excavation in the tunnel (outside the tunnel-viaduct interaction zone), the karstic cavity encountered at a depth of approximately 2–3 m and in the form of a cony was filled with concrete (Fig. 7).

Contour diagrams of the discontinuities were drawn by measuring the locations of 53 discontinuities from the dolomitic limestone units known to contain karstic voids, which have been encountered in the interaction zone of the T5-1 Tunnel and Osmangazi Bridge Approach Viaducts. Accordingly, the bedding dominant orientation is 12/106

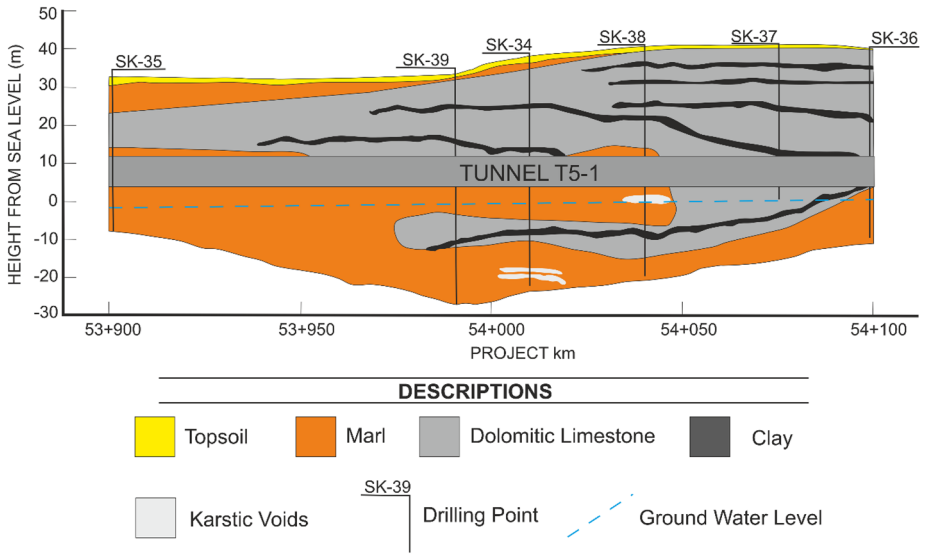

Fig. 5 Geological section of T5-1 Tunnel

Table 1 Physico-mechanical and elastic properties of rock samples belonging to geotechnical units [22]

Physico-mechanical and elastic properties		Dolomitic limestone (n = 13)	Marl (n = 7)
Unit weight (kN/m^3)	Max	2.81	2.8
	Min	2.54	2.56
	Average	2.59	2.63
Uniaxial Compressive strength (MPa)	Max	76.95	59.01
	Min	20.71	14.7
	Average	49	34
Deformation modulus (GPa)	Max	16.89	17.12
	Min	5.79	6.02
	Average	6.46	12.3
Poisson's ratio	Max	0.24	0.3
	Min	0.2	0.2
	Average	0.22	0.24

(dip/dip direction) and the bidirectional discontinuity system is 69/228, 75/277. It also has irregularly oriented discontinuities (Fig. 8).

When the regular and irregular discontinuities (discontinuities and beddings) in the dolomitic limestones are evaluated together, it is thought that they can control the formation of karstic caves that cannot be followed within the unit due to their long continuity and cross-cutting positions.

Methodology

The permissible value for vertical deformation in the Osman Gazi Tunnel approach viaducts has been reported by the Turkish Highways Authority as 25 mm, and the deformation limit value in the direction parallel to the highway axis is 5 mm. In order not to exceed

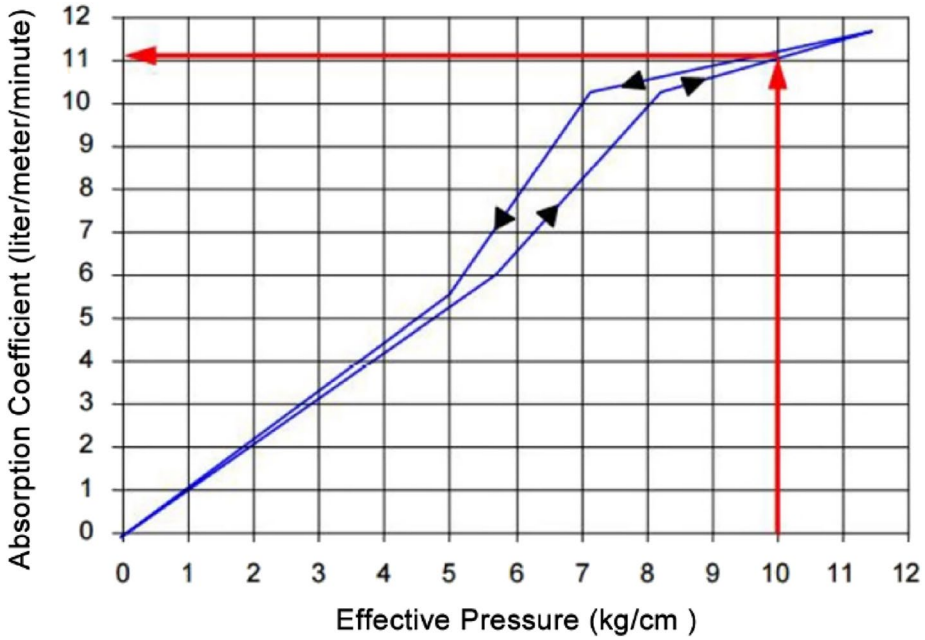

Fig. 6 Determination of Lugeon value in SK-36 borehole by graphical method

Fig. 7 Karst cave encountered during tunnel excavation in dolomitic limestones

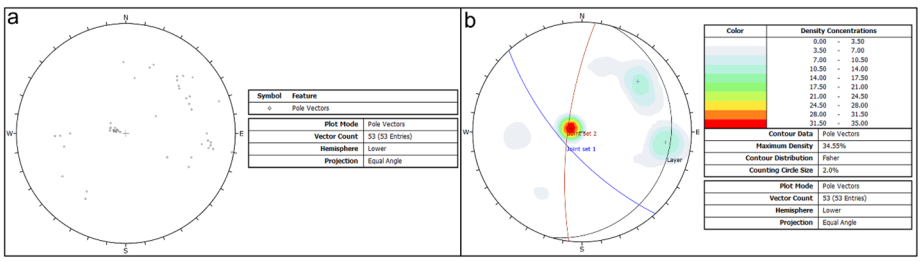

Fig. 8 Pole points (**a**) and contour diagram (**b**) of discontinuity and layer measurements

these limit values, tunnel support works are divided into 2 stages in order to minimize the structure-tunnel interaction in the T5-1 Tunnel. In the first stage, the injection was projected to fill the cavities and increase the strength of the rock mass. Then, the tunnel excavation and rigid support system were planned.

Grouting

Grouting is critically important in tunnel engineering. The compaction grouting mode or hydro-fracture grouting mode can be used depending on the local geological conditions of the given project [52]. To date, the majority of grouting applications have adopted the soil fracture technique [47]. However, as grouting is a complex process, both permeation grouting and compaction grouting can be observed in a fracture grouting-dominated process. Many factors may affect the eventual grouting modes used, such as the grout material, grouting pressure, soil type, and stress state of the ground [36].

Superficial injection method was chosen for the injection process to be applied to fill the discontinuities and karstic voids, which are quite complicated, due to the shallowness of the tunnel instead of the tunnel. In an area of 87 m in length and 27 m in width where the T5-1 Tunnel interacts with the Osman Gazi Bridge approach viaducts, injection wells with a depth of 33 m to 55 m were determined in a 3 m grid (278 wells) (Fig. 9).

Equation 1 was used to calculate the pressure to be applied in consolidation injections while Eq. 2 was employed in order to prevent negative effects in loose material and shallow parts of wells. Equation 3 was used for pressure monitoring during the injection process.

$$Pt = 2 + 0.33\ H \tag{1}$$

$$Pt = 2 + 0.23\ H \tag{2}$$

$$Pm = Pt - (w \times H \times \cos a)/10 \tag{3}$$

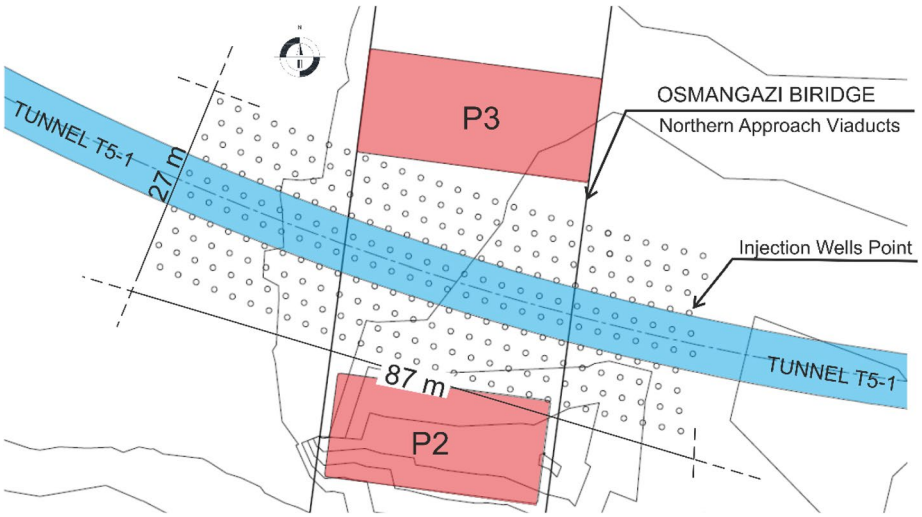

Fig. 9 Layout of injection wells on the T5-1 Tunnel route (Prohit [46]

where, P_t: Total effective pressure applied to the stage (kg/cm^2); P_m: Pressure that should be read on the manometer (kg/cm^2); H: The distance of the midpoint of the injected stage to the well mouth (m); w: Specific gravity of injection material (gr/cm^3); α: Angle of the well with vertical.

In the pressurized water tests to be performed in the control wells to be opened after the consolidation injection is completed, the water leakage amount (injection pressure) was checked with Eq. 4 and the permeability was determined.

$$Q/(P \times L \times t) < 1 \text{ (10 Lugeon)} \tag{4}$$

where Q: Total amount of water leakage in the stage (l); P: The total pressure applied in the test stage (kg/cm^2); L The length of the test stage (m); t Test duration (min).

The determination of the injection mixture to be used in filling the karstic voids and the follow-up of the process are extremely important in terms of both cost and void filling efficiency. Adjusting the appropriate viscosity value and setting time according to the state of the voids in the mixture increases the injection efficiency. For this reason, 7 different mixtures were formed to be adjusted in the field according to the amount of flow in the injection wells (from more fluid to less fluid) (Table 2).

Before starting the injection process, bentonite was mixed with water at a ratio of 1/10 and allowed to rest for 24 h, and then added to the mixture. The prepared injection mixture was used within 2 h. Hole diameters are 60 mm, injection process was started with grout number 1 and 1 m^3 was given first. Then, the pressure values in each well were monitored in a controlled manner and the mixtures numbered 2, 3, 4, and 5 were passed. However, when the expected reflux could not be obtained in mixture number 7, the injection process was interrupted and the material was expected to set. In total 22,567 tons of mixture were injected into 278 wells.

Drilling and geophysical studies were carried out in the field in order to measure the success of the grouting methodology applied before the start of tunnel construction works.

Table 2 Injection grout mixing ratios (CEM II –A of cement, gradation of TSE EN ISO 13500 sand: 95% must pass through sieve no 16, 50% sieve no 50 and 5% < sieve no 200, specific gravity should be > 2 gr/cm^3; Prohit [46]

Mix No	Mixing rate	Cement (kg)	water (lt)	Sand (%)	Bentonite (kg) %	Specific gravity (gr/cm^3)
1	1/1	150	150	–	1	1.5
2	10/9	167	150	–	1	1.54
3	5/4	187.5	150	–	1	1.58
4	7/5	210	150	–	1	1.63
5	7/5	210	150	25	1	1.65
6	7/5	210	150	50	1	1.67
7	7/5	210	150	100	1	1.69

Drillings

After the completion of the grouting processes, 3 core drillings with a depth of 50 m were drilled and a PWT test was carried out at 3 m. According to the PWT results, all wells were measured as impermeable. It was observed that the injection spread and filled the voids in the 50 m deep well VA25 at 26.80 m, 28.00 m, 29.80 m, 33 m, 33.30 m, 34.30 m, and 35.70 m (Fig. 10).

Electrical resistivity tomography (ERT)

Electrical resistivity tomography (ERT) method was used to determine how effective the injection studies on the T5-1 Tunnel were. For ERT studies, 4 profile resistivity tomography lines were determined and these lines were measured with 110 m profile length, 56 electrodes and dipole–dipole expansion. In Fig. 11, the resistivity inversion section of the ERT-1 line is given.

As seen in Fig. 11, the red-colored area indicates that the injection has fully penetrated, and the blue and green-colored areas show the areas where the injection has not penetrated. Areas, where the grout does not penetrate, were detected locally between 4 and 52 m of the profile length, between 2 and 10 m depths, between 5 and 18 m depths at 58–70 m of the profile length and between 78 and 96 m of the profile length at 5–28 m depths. It turned out that these areas should be filled by opening injection wells again.

Seismic measurements

Seismic studies by using the MASW method between the P-02 and P-03 piers of the northern approach viaduct were performed, and hence, seismic refraction and profiles were prepared (Fig. 12).

The elastic parameters of the units forming the study area, the dominant period of the ground, and the ground amplification value were determined by seismic measurements.

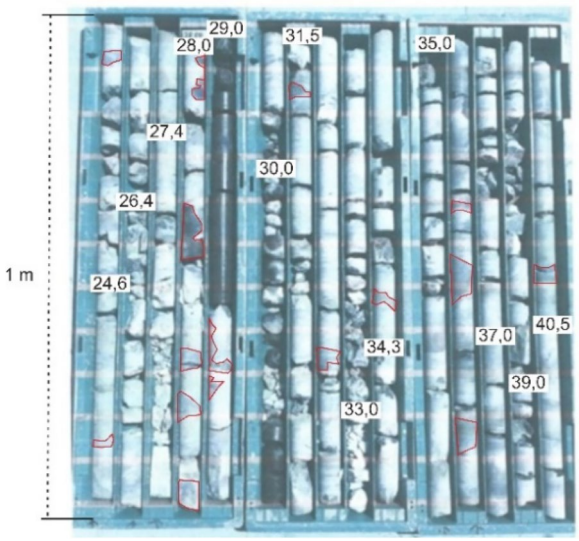

Fig. 10 Injection spread in borehole VA25 (areas within the red lines indicate injection, the tunnel is between 28–35 m)

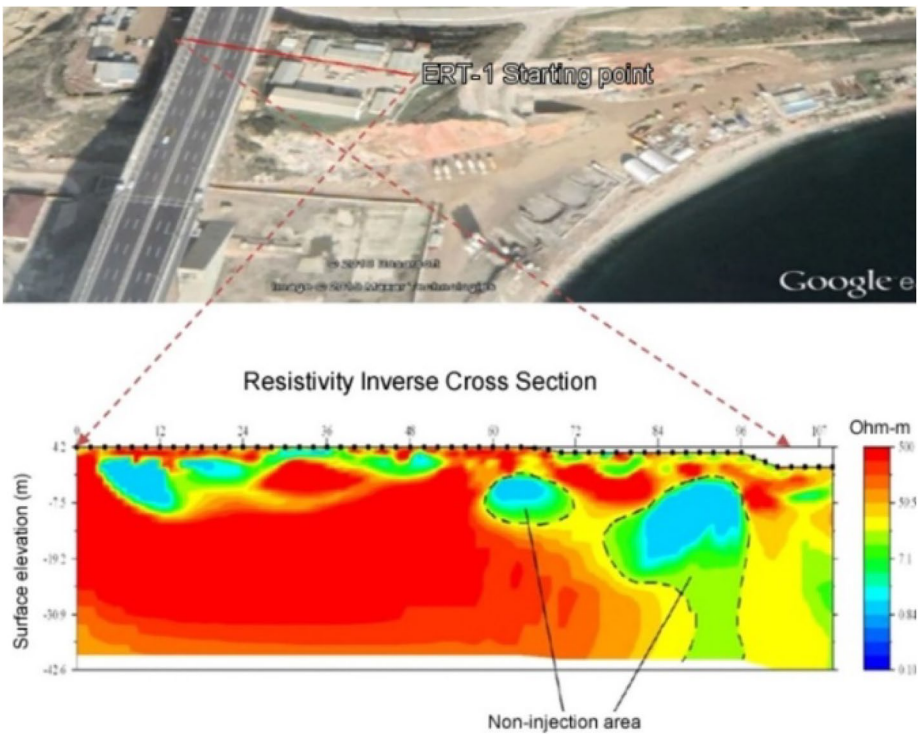

Fig. 11 ERT-1 Line Resistivity inversion section

Fig. 12 Distribution of the MASW measurement point over the tunnel

2 seismic lines were determined, these areas are above the T5-1 tunnel where the injection was performed and between the piers of the Viaduct P-02 and P-03.

In the first seismic refraction data, the section length is 39.0 m, and a low-velocity unit was detected in the section between 27.0 m and 39.0 m and up to 7.0 m in depth. When the MASW measurement along the profile was evaluated, a joint or discontinuity system was detected between 4.50 m and 7.50 m at a depth of 13.0 m. In the second seismic refraction data, the section length is 52.0 m and it was seen that there is a low-velocity unit between 40.0 m and 52.0 m and at a depth of 7.50 m. In this part, when the MASW measurement was evaluated, no discontinuity or joint system was detected. In this part, it was understood that the grout penetrated the rocks and filled the voids.

For the first profile, the average shear wave velocity (V_{s30}) was obtained as 1066 m/sec for the 30 m depth, and the ground dominant period (T_0) is 0.17 s at the measurement elevation in the field. For the Second Profile, the average shear wave velocity (V_{s30}) is determined as 1034 m/sec for the 30 m depth, and the ground dominant period (T_0) is 0.18 s at the measurement elevation in the field. Considering these data, it was understood that the effective ground acceleration (a_{max}) in the field should be used as 0.592 g.

Injection propagation in tunnel excavation face

By using the time optimally, the excavation and support works in the part of the tunnel that will be passed without injection were performed from the tunnel exit to the entrance. In the tunnel excavation faces at the entrance of the injected area, the injection spread is mostly in the form of filling the karstic spaces (Fig. 13a), there is no order or discontinuity tracking. Injections filled large karst cavities. As the tunnel approaches the region of the viaduct piers, the injection spreads along the karst cavity and discontinuity surfaces (Fig. 13b). In the tunnel viaduct region (Fig. 13c) and its continuation (Fig. 13d), injection appears to be completely under discontinuity control. In this case, it shows parallelism with the research studies carried out both before and after the injection procedure. In addition, it has been understood that the methodology applied for the grouting process in the excavations in the tunnel yielded very successful results.

Fig. 13 Injection dispersions encountered during tunnel excavation (a-Km:54 + 049,00, b-Km: 54 + 028.25, c-Km: 54 + 004.25, d-Km:53 + 990.75 excavation face, injection are the areas within the yellow lines)

Support system design at viaduct region

The tunnel interacts with the viaduct piers between Km: 53 + 980 − 54 + 060 (80 m). In this region, the distance from the Bridge side piers to the nearest bored pile is 22.90 m for the P-02 pier and 21.27 m for the P-03 pier (See Fig. 2). Determining the tunnel support to be applied after the injection process is important in terms of minimizing the viaduct—tunnel interaction and getting the highest performance from the support.

There are basically 3 main approaches to determine tunnel support systems such as empirical methods, analytical methods, and numerical methods [6]. Empirical methods include the rock mass classification systems. Several rock mass classification systems have been developed since the pioneering study by Terzaghi [55] involving a rock load factor classification [61]. The rock mass rating (RMR) and NGI tunneling quality index (Q) are the most applied and accepted systems worldwide. The RMR classification was proposed in 1973 as a jointed rock mass classification system [12], and major revisions were performed in 1989 and 2014 [13, 15]. The Q-system was developed in 1974 [11], and major changes in characterization and classification were proposed in 1993 and 2002 [10, 30]. The Q-system was developed based on the tunneling cases for hard and jointed rock masses [45]. Both classification systems are inappropriate for the tunnel support design in highly stressed jointed rock mass, and this is the limitation of the data on which these systems are based [48]. Analytical methods were developed by various researchers [21, 31, 54, 62]. In analytical methods, the medium is considered as homogeneous and isotropic. In other words, all studies are performed in an idealized environment. However, the units tunnel passes through during the application phase are not isotropic and homogeneous. For this reason, analytical solutions have limitations [5]. Numerical analysis methods are the main methods used to determine tunnel support systems [1, 2, 6–8, 38, 50, 51, 58, 59]. Decisions based on practice and experience are essential in determining support systems, and numerical analyzes can be considered as a guide to practical decisions. Some numerical modelling methods are the finite element method, discrete element method and finite difference method. Among these methods, the finite element method is one of the most successful methods for anisotropic and nonlinear environments [60].

Numerical modeling

As mentioned before, an interaction between the bridge and the tunnel is possible. To understand this interaction, 2 and 3 dimensional modelings are carried out. The NATM class of the interaction zone is B3. In the interaction zone, the excavation stage at upper bench is selected as 1.25 while that at lower bench is considered as maximum 2.5 m. As the support elements, NPI140 steel shoring, f28 SN (Store Norfors) rockbolts with 1.5 × 1.5 m pattern and 1.5″ forepooling with 40 cm interval are used. In addition, double layers Q589/478 steel mesh and 20 cm shotcrete are applied. When selecting these elements, the principles of the New Austrian Tunneling Method (NATM) are employed. The 2D (Rocscience Phase 2D V8.2) 3D numerical analyses (Midas GTS NX) were performed by Emre Özcan Engineering [22].

Table 3 Material parameters used in the numerical analysis [22, 46]

Parameters	Dolomitic limestone	Tunnel liner shotcrete		Steel (Steel profile/Bolt/ Forepool)
		Unhardening	Hardening	
Deformation modulus, E (MPa)	646.4	1700	17,000	2100000
Unit Weight (kN/m^3)	2.59	24.0	24.0	78.5
Poisson's ratio	0.22	0.20	0.20	0.15
Material model	Generalized Hoek Brown	Elastic		
Initial m_b	0.981333			
Initial s	0.00073			
Initial a	0.51595			
Residual m_b	0.981333			
Residual s	0.00073			
Residual a	0.51595			
Uniaxial compressive strength, (MPa)	34			
Dilatancy Angle,^{0}	21			

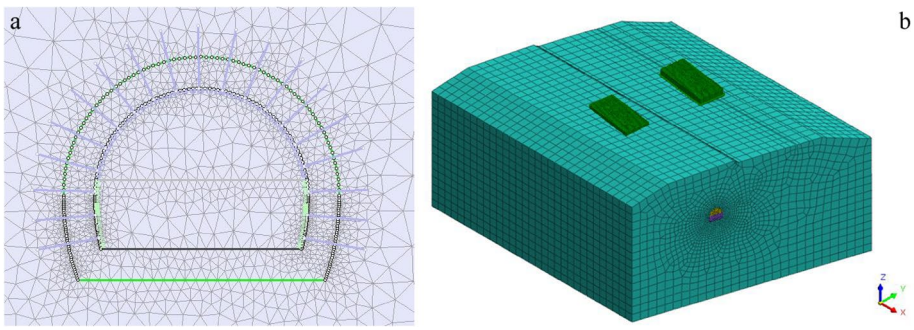

Fig. 14 Numerical mesh model for T5-1 Tunnel and Osmangazi approach viaduct interaction (**a**: 2D model (Rocscience Phase 2D V8.2), **b**: 3D model (Midas GTS NX) were performed by Emre Ozcan Engineering and Prohit Engineering [22, 46]

Results of the numerical analyses

The maximum stresses created by the viaduct piers is 1000 kPa. The parameters of the rock mass and support elemens are given in Table 3. 2 and 3 D model prepared by [22] is shown in Fig. 14. 2D models for 3 different critical sections (Km: 54 + 013, 54 + 024, 54 + 035) in 6 steps (1-location of stresses in place, 2-excavation of the upper half, 3-installation of the support system, 4-installation of the lower half, 5 -installation of the support lower half, 6-tunnel lining construction and earthquake situation) are performed. The dimensions of the 3D models are 154 m × 147 m × 76 m, and the analyses are performed for all construction stages (96 stage). In the last stage, the peak ground acceleration is considered as 0.488 g. In this stage, as the support elements, only the lining concrete is used.

By fininte element analyses, not only tunnel deformation, shoring effects and deformation of viaduct foundation but also maximum effects on foundation piles of the viaduct, deformation of tunel lining and axial forces on rockbolts are assessed. The total deformations for the seismic conditions are shown in Fig. 15. According to the results of the

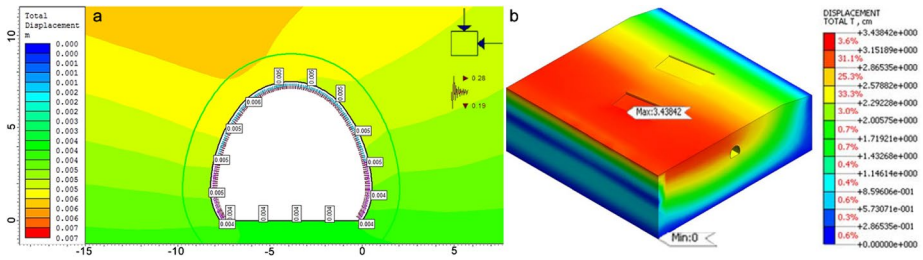

Fig. 15 Total displacement in 2D and 3D numerical analysis for pseudo-static conditions (**a**: 2D Rocscience Phase 2D V8.2), **b**: 3D (Midas GTS NX) were performed by Emre Ozcan Engineering and Prohit Engineering [22, 46]

analyses, the maximum deformation of the tunnel lining is 2.91 mm while that of the viaduct foundations is 0.9 mm.

According to the results of the pseudo-static analyses, the maximum defomation in the interaction zone is obtained as 4.2 mm for ceiling of the tunnel and 6.8 mm for invert of the tunnel. The maximum deformation for the viaduct foundations is calculated as 3 mm. All results obtained from the numerical analyses are summarized in Table 4.

When Table 4 is examined carefully, according to the results of the 2D numerical analysis, deformation of 10 mm in the vertical direction (5 mm in 3D calculations) is calculated in the tunnel due to excavations in static conditions under the grouted rock conditions. It is observed that the effects of these deformations on tunnel and viaduct foundations are in the order of 1–2 mm in the static condition. In case of earthquake, 5–6 mm vertical deformation and 12–14 mm horizontal deformation values in the tunnel lining are calculated. It is calculated as 2 mm due to more representative conditions in 3D calculations. In addition, deformations of 4–5 mm of the viaduct foundation and piles are obtained in the earthquake conditions. Consequently, all deformations obtained from the numerical analyses are negligible and the grouting provides an important improvement on the rock mass. In addition, it is almost impossible to describe the distribution and the dimensions of the karstic voids along the T5-1 tunnel route. The karstic caves are filled by grouting and hence, the possible negative effects of the caves are eliminated. For this reason, during the analyses, the caves are not considered.

Monitoring results

Due to the interaction of the T5-1 tunnel and the Osman Gazi Bridge's approach viaducts, it is obligatory to monitor the deformations in the tunnel and on the viaduct. For this reason, a continuous monitoring system is set up with precise measuring instruments inside the tunnel and on the viaduct during the tunnel construction.

Measurements inside the tunnel

In-tunnel measurements are made on the basis of monitoring the deformations of the points placed on the supporting elements [39]. Tunnel monitoring data (convergence) gives serious information about tunnel conditions [33]. In order for the T5-1 Tunnel to be excavated safely and, progress can be achieved, the critical basic value was determined as 5 mm, the indicator level 7 mm, and the alarm level 10 mm with numerical

Table 4 2D and 3D Numerical Analysis Results [22, 46]

Phase 2D/Midas (G) analysis sections	**2D analysis section-1**		**2D analysis section-2**		**2D analysis section-3**		**3D analysis section**	
Section (km)	**54 + 013**		**54 + 024**		**54 + 035**		**53 + 900 − 54 + 160**	
Construction/analysis phase	Post construction (NATM excavation static conditions)	Earthquake condition (permanent lining)	Post construction (NATM excavation static conditions)	Earthquake condition (earthquake condition after permanent lining)	Post construction (natm excavation static conditions)	earthquake condition (earthquake condition after permanent lining)	Post construction (NATM excavation static conditions)	Earthquake condition (earthquake condition after permanent lining)
Tunnel roof displacement dy[a] (mm)	− 6.9	3.3	− 9.8	3.5	− 9.9	3.8	− 4.2	0.05
Tunnel base displacement dy (mm)	9.5	1.6	7.1	1.6	7.6	2	6.8	− 0.6
Viaduct foundation displacement dy (mm)	− 1.2	4.5	− 1.2	4.9	− 1.5	5	− 0.9	4.5
Viaduct pile displacement dy (mm)	− 1.1	4.4	− 1.2	4.8	− 1.4	4.9	− 0.8	3.8
Tunnel temporary lining displacement (mm)	− 7.2	0	− 7.3	0	− 7.8	0	− 4.2	0
Tunnel temporary lining displacement x[c] (mm)	1.9	0	1.9	0	1.8	0	0.6	0
Tunnel temporary lining max. moment, M (kNm/m)	32.7	0	27.7	0	27.9	0	11.3	0
Tunnel temporary lining max. shear force Q[b](kN/m)	140.6	0	152.6	0	146.5	0	61.4	0
Rock bolt load (kN/m)	66.2	0	67.6	0	68.2	0	0	0
Rock bolt load (kN)	82.7	0	84.5	0	85.3	0	91	0

Table 4 (continued)

Phase 2D/Midas (G) analysis sections	2D analysis section-1		2D analysis section-2		2D analysis section-3		3D analysis section	
Section (km)	**54 + 013**		**54 + 024**		**54 + 035**		**53 + 900 − 54 + 160**	
Tunnel permanent lining displacement dy[d] (mm)	0	5.2	0	5.8	0	6	0	2
Tunnel permanent lining displacement dx[d] (mm)	0	Ad = 70–58 = 12	0	Ad = 72–59 = 13	0	Ad = 74–60 = 14	0	Ad = 29–27 = 2
Tunnel permanent lining max. moment, M (kNm/m)	61	157.1	58.2	162.7	59.7	172.7	11.3	57.5
Tunnel permanent lining max. shear force, Q (kN/m)	58.5	91.4	52.9	95.1	57.5	102.4	61.4	84.4

[a] (−) dy values are settlement, (+) dy values are swelling

[b] (+) dx values are the covergence values towards the tunnel

[c] The high values obtained for the static situation in 2-dimensional analyzes are the peak values of the support region

[d] In the permanent coating phase, which was completed after the NATM excavation works, the deformations were zeroed so that the earthquake effects could be seen

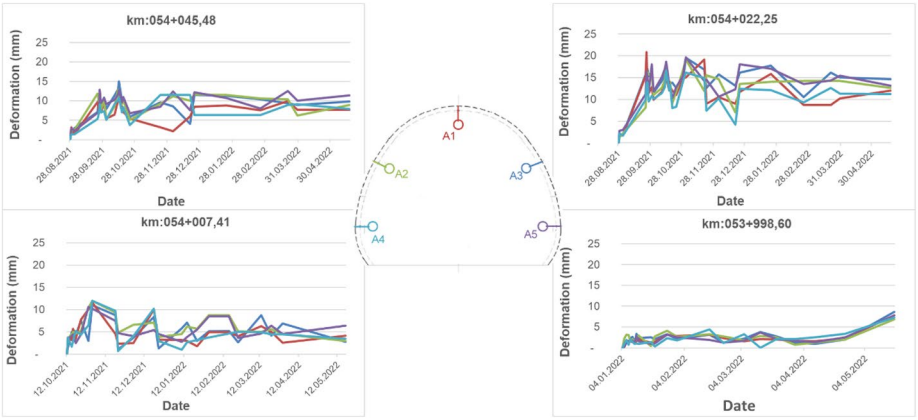

Fig. 16 Deformation monitoring points and measurement graphs

Fig. 17 Readings dated (01.06.2022) after the completion of the tunnel from tiltmeters and ODSs placed on Viaduct P-02 and P-03 legs (Orange dots show Tilt Meters, green dots show ODS points, yellow arrows show the direction of movement)

analysis. The optotigonometric method is preferred to determine the deformations in the tunnel and 5 optical prisms are placed every 5 m in the tunnel (Fig. 16). By monitoring the daily deformations in the tunnel, weekly and monthly measurements are decided, and it is understood that the measurements are slightly better than the threshold values predicted for the tunnel (Fig. 16).

Measurements on the viaduct

Inclinometer (tiltmeter) and optical deformation sensor (Optical Displacement Sensor-ODS) monitoring system are installed for instant data recording on the Osmangazi Bridge North approach viaduct P-02 and P-03 piers. This setup is followed instantly via the cloud system.

On the bridge piers, the pier on the right side is 4,5 and 6, and ODS 4,5 and 6 are located on the P-02 pier, and the left pier is the P-03 (with Tilt 1, 2 and 3 and ODS 1, 2

and 3). The graph of these oscillations are read and evaluated on tiltmeters is given in Fig. 17.

There are 25 mm limit values for vertical deformation in bridge piers and 5 mm limit values for deformations parallel to the highway axis. In the measurements performed, values of 4.9759 mm in Tilt 1 and 4.3102 mm in Tilt 4 are read, and it is understood that the tunnel-viaduct interaction remains within the limit values by following the effects of vibration during excavations and the oscillations caused by the traffic on the Bridge (Fig. 18).

Conclusions

Structure-tunnel interaction is extremely important in tunnels excavated in rocks containing karstic cavities as well as weak rock or soil tunnels. In this study, the T5-1 Tunnel passing between the Osmangazi Bridge North approach viaduct P-02 and P-03 piers in the Gebze-Köseköy Railway Project is investigated in terms of structure-tunnel interaction.

In the T5-1 Tunnel design phase, research and test procedures are established to investigate the karstic cavities before starting the construction process and to estimate the extent of these cavities. Since these cavities pose a risk during tunnel construction, it is decided to apply injection, and injections are performed in 7 different injection mixtures and 4 different pressure phases.

The consolidation injection for filling the karstic cavities contributed to the acceptance of the rock environment as homogeneous and isotropic in numerical analysis. In addition, by filling the karstic voids, it prevents possible asymmetrical loads on the tunnel lining.

The injection creates a shell cover for the tunnel construction excavation and filled the discontinuities in the rock mass, eliminating the negative conditions that could cause excessive breakage, and allowing the tunnel to be excavated safely.

As another way to minimize structure-tunnel interaction, a fast-forming and relatively rigid tunnel support were modeled with 2D and 3D FEM instead of a flexible shell. Measurements taken from the tunnel and viaducts and, deformations calculated with 2D and 3D numerical models were compared. As a result of this comparison, it is understood that the measurement results give close results to the 3D numerical analysis results. For

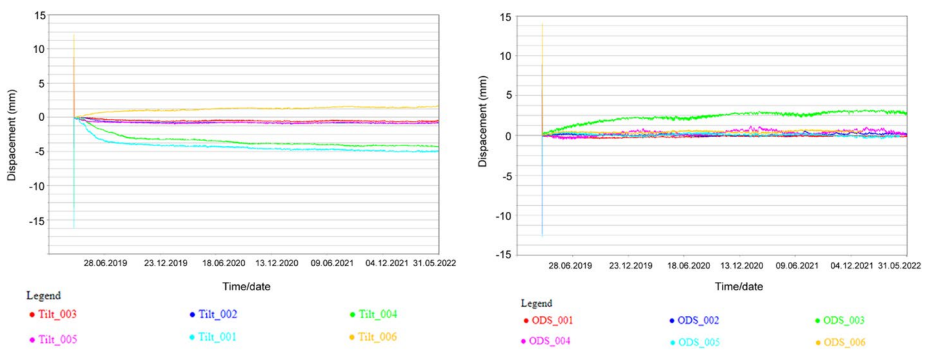

Fig. 18 Tiltmeter and ODS graphics placed on the Viaduct P-02 and P-03 piers

example, the maximum deformation is measured as 2.54 mm while this value is obtained as 3 mm from the 3D numerical analyses.

Finally, the tunnel was completed without any problems.

Acknowledgements
The authors thank to General Directorate of Türkiye Railway System for continuous support.

Author contributions
GT performed intial project design, calculations, grouting works and initial draft of the manuscript; EP performed all monitoring studies, observations on tunnel construction stage and writing manuscript; CG performed design, conceptualism and monitoring works, calculations, monitoring, manuscript writing and editing. All authors read and approved the final manuscript.

Declarations

Competing interests
The authors declare that they have no conflict of interest.

Received: 3 November 2022 Accepted: 6 February 2023
Published online: 10 March 2023

References

1. Akgün H, Muratlı SW, Kockar MK (2014) Geotechnical investigations and preliminary support design for the Gecilmez tunnel: a case study along the Black Sea coastal highway, Giresun, Northern Türkiye. Tunn Undergr Space Technol 40:277–299
2. Aksoy CO, Ogul K, Topal I, Ozer SC, Ozacar V, Posluk E (2012) Numerical modeling of non-deformable support in swelling and squeezing rock. Int J Rock Mech Min Sci 52:61–70. https://doi.org/10.1016/j.ijrmms.2012.02.008
3. Alija S, Torrijo FJ, Quinta-Ferreira M (2013) Geological engineering problems associated with tunnel construction in karst rock masses: the case of Gavarres tunnel (Spain). Eng Geol 157:103–111. https://doi.org/10.1016/j.enggeo.2013.02.010
4. Altınlı İE, Soytürk N, Saka K (1970) Hereke-tavşancıl-tavşanlı-tepecik alanının jeolojisi. İstanbul Üniversitesi Fen Fakültesi Mecmuası 35:69–75
5. Aygar EB (2022) Methods used in tunnel design (Empirical, analytical and numerical methods), limitations, comparison and suggestions. Railw Eng 15:125–133. https://doi.org/10.47072/demiryolu.1030404
6. Aygar EB, Gokceoglu C (2021) Effects of portal failure on tunnel support systems in a highway tunnel. Geotech Geol Eng 39(8):5707–5726. https://doi.org/10.1186/s40703-021-00142-7
7. Aygar EB, Gokceoglu C (2021) Analytical solutions and 3D numerical analyses of a shallow tunnel excavated in weak ground: a case from Turkey. Int J Geo-Eng 12:9. https://doi.org/10.1186/s40703-021-00142-7
8. Aygar EB, Karahan S, Gullu S, Gokceoglu C (2022) Analytical and numerical analyses of the support system for a large-span tunnel in challenging and seismically active ground conditions. Geotech Transp Infrastruct. https://doi.org/10.1007/s40515-022-00251-5
9. Bakalowicz M (2005) Karst groundwater: a challenge for new resources. Hydrogeol J 13(1):148–160
10. Barton N (2002) Some new Q-value correlations to assist in site characterisation and tunnel design. Int J Rock Mech Min Sci 39:185–216
11. Barton N, Lien R, Lunde J (1974) Engineering classification of rock masses for the design of tunnel support. Rock Mech 6:189–236
12. Bieniawski ZT (1973) Engineering classification of jointed rock masses. Civil Engineering= Siviele Ingenieurswese 12:335–343
13. Bieniawski ZT (1989) Engineering rock mass classifications: a complete manual for engineers and geologists in mining, civil, and petroleum engineering. John Wiley & Sons, New York
14. Boscardin MD, Cording EJ (1989) Building response to excavation-induced settlement. J Geotechn Eng 115(1):1–21
15. Celada B, Tardáguila I, Varona P, Rodríguez A, Bieniawski Z T (2014) Innovating tunnel design by an improved experience-based RMR system. 40th World Tunnel Congress 1–9
16. Chen F, He C, Li X, Wang B (2020) Construction schemes for shallow and asymmetrically loaded tunnels crossing below a bridge. Int J Geomech 20(7):04020098. https://doi.org/10.1061/(ASCE)GM.1943-5622.0001653
17. Chen YF, Liao Z, Zhou JQ, Hu R, Yang Z, Zhao XJ, Yang XL (2020) Non-darcian flow effect on discharge into a tunnel in karst aquifers. Int J Rock Mechan Mining Sci 130:104319. https://doi.org/10.1016/j.ijrmms.2020.104319
18. Devriendt M, Williamson M (2011) Validation of methods for assessing tunnelling-induced settlements on piles. Ground Eng. 12:25–30
19. Dias TGS, Bezuijen A (2015) Data analysis of pile tunnel interaction. J Geotech Geoenviron Eng 141(12):04015051. https://doi.org/10.1061/(ASCE)GT.1943-5606.0001350
20. Dimmock PS, Mair RJ (2008) Effect of building stiffness on tunnelling-induced ground movement. Tunn Undergr Space Technol 23(4):438–450
21. Hoek E, Brown ET (1988) The Hoek-Brown failure criterion—A 1988 update. 15th Canadian Rock Mechanics Symposium, 31–38
22. Emre Özcan Engineering (2017) T5–1 Tunnel Account Report. Internal project report, p 290 (unpublised)

23. Emre Ö, Doğan A, Duman TY, Özalp S (2011) 1:250,000 Scale Active Fault Map Series of Turkey, Bursa (NK35–12) Quadrangle. Serial Number: 9, General Directorate of Mineral Research and Exploration, Ankara-Turkey (unpublised)
24. Eroskay, SO (1975) The hydrogeology of the limestones in the south of Kocaeli peninsula and the analysis of karst parameters. The Scientific and Technical Research Council of Türkiye, TBAG-124 project (unpublised)
25. Farrell R, Mair R, Sciotti A, Pigorini A (2014) Building response to tunnelling. Soils Found 54(3):269–279
26. Franza A, Marshall AM, Haji T, Abdelatif AO, Carbonari S, Morici M (2017) A simplified elastic analysis of tunnel-piled structure interaction. Tunn Undergr Space Technol 61:104–121
27. Franzius JN, Potts DM, Burland JB (2006) The response of surface structures to tunnel construction. Proc ICE Geotech Eng 159(1):3–17
28. Garner C, Coffman R (2013) Subway tunnel design using a ground surface settlement profile to characterize an acceptable configuration. Tunn Undergr Space Technol 35:219–226
29. Giardina G, DeJong MJ, Mair RJ (2015) Interaction between surface structures and tunnelling in sand: centrifuge and computational modelling. Tunn Undergr Space Technol 50:465–478
30. Grimstad E, Barton N (1993) Updating the Q-system for NMT. In: Proc. Int. Symp. On sprayed concrete-modern use of wet mix sprayed concrete for underground support 46–66
31. Hoek E, Brown ET (2019) The hoek-brown failure criterion and GSI–2018 edition. J Rock Mechan Geotechn Eng 11(3):445–463. https://doi.org/10.1016/j.jrmge.2018.08.001
32. Huang M, Zhang C, Li Z (2009) A simplified analysis method for the influence of tunneling on grouped piles. Tunn Undergr Space Technol 24(4):410–422
33. Incecik M, Poşluk E (2018) Tunnel T26 on the Ankara-Istanbul high speed rail route–Tunnelling under difficult conditions: Der Tunnel T26 auf Schnellstrecke Ankara–Istanbul–Vortrieb unter schwierigen geologischen Verhältnissen. Geomechanics and Tunnelling 11(5):434–440. https://doi.org/10.1002/geot.201800026
34. Jacobsz SW, Standing JR, Mair RJ, Hagiwara T, Sugiyama T (2004) Centrifuge modelling of tunnelling near driven piles. Soils Found 44(1):49–56
35. Kaalberg FJ, Teunissen EAH, van Tol AF, Bosch JW (2005) Dutch research on the impact of shield tunnelling on pile foundations. In: Bakker KJ, Bezuijen A, Broere W, Kwast EA (eds) Proceedings of the 5th International Symposium on Geotechnical Aspects of Underground Construction in Soft Ground. Taylor & Francis, Amsterdam, pp 123–131
36. Kayabasi A, Gokceoglu C (2019) An assessment on permeability and grout take of limestone: a case study at Mut Dam, Karaman. Turkey Water 11:2649. https://doi.org/10.3390/w11122649
37. Kitiyodom P, Matsumoto T, Kawaguchi K (2005) A simplified analysis method for piled raft foundations subjected to ground movements induced by tunnelling. Int J Numer Anal Meth Geomech 29(15):1485–1507
38. Koçkar MK, Akgün H (2003) Methodology for tunnel and portal support design in mixed limestone, schist and phyllite conditions: a case study in Türkiye. Int J Rock Mech Min Sci 40:173–196
39. Kovari K, Amstad C (1993) Decision making in tunnelling based on field measurements. In: Hudson J (ed) Comprehensive rock engineering, vol 4. Pergamon, Oxford, pp 571–605
40. Maleki M, Sereshteh H, Mousivand M, Bayat M (2011) An equivalent beam model for the analysis of tunnel-building interaction. Tunn Undergr Space Technol 26(4):524–533
41. Marshall A, Mair R (2011) Tunneling beneath driven or jacked end-bearing piles in sand. Can Geotech J 48(12):1757–1771
42. Marshall AM, Haji T (2015) An analytical study of tunnel-pile interaction. Tunn Undergr Space Technol 45:43–51
43. Melis M, Medina L, Rodríguez J (2002) Prediction and analysis of subsidence induced by shield tunnelling in the madrid metro extension. Can Geotech J 39(6):1273–1287
44. Ng CWW, Lu H, Peng SY (2012) Three-dimensional centrifuge modelling of the effects of twin tunnelling on an existing pile. Tunn Undergr Space Technol 35:189–199. https://doi.org/10.1016/j.tust.2012.07.008
45. NGI (2015) Using the Q-system rock mass classification and support design. Allkopi AS, Oslo
46. Prohit Engineering (2017) Km: 53+930.000-Km: 54+160.000 T5–1 Tunnel ınjection wells project Ankara pp. 25 (unpublised)
47. Essler R, Drooff E, Falk E (2000) Compensation grouting: concept, theory and practice advances in grouting and ground modification. American Society of Civil Engineers, Reston, pp 1–15
48. Rehman H, Naji AM, Kim JJ, Yoo H (2019) Extension of tunneling quality index and rock mass rating systems for tunnel support design through back calculations in highly stressed jointed rock mass: an empirical approach based on tunneling data from Himalaya. Tunn Undergr Space Technol 85:29–42. https://doi.org/10.1016/j.tust.2018.11.050
49. Reimann T, Rehrl C, Shoemaker WB, Geyer T, Birk S (2011) The significance of turbulent flow representation in single-continuum models. Water Resour Res 47:W09503. https://doi.org/10.1029/2010WR010133
50. Rinaldi AP, Urpi L (2020) Fault reactivation induced by tunneling activity in clay material: hints from numerical modeling. Tunell Undergr Space Technol 102:103453. https://doi.org/10.1016/j.tust.2020.103453
51. Shi YF, Fu JY, Yang JS, Xu CJ, Geng DX (2017) Performance evaluation of long pipe roof for tunneling below existing highway based on field tests and numerical analysis: case study. Int J Geomech 17(9):04017054. https://doi.org/10.1061/(ASCE)GM.1943-5622.0000933
52. Soga K, Au SKA, Jafari MR, Bolton MD (2004) Laboratory investigation of multiple grout injections into clay. Geotechnique 54(2):81–90
53. Soomro MA, Hong Y, Ng CWW, Lu H, Peng S (2015) Load transfer mechanism in pile group due to single tunnel advancement in stiff clay. Tunn Undergr Space Technol 45:63–72. https://doi.org/10.1016/j.tust.2014.08.001
54. Sulem J, Panet M, Guenot A (1987) An analytical solution for time-dependent displacements in a circular tunnel. Int J Rock Mech Min Sci Geomech Abstr 24(3):155–164
55. Terzaghi K (1946) Rock defects and loads on tunnel supports. In: Proctor RV, White TL (eds) Rock tunneling with steel supports, vol 1. Commercial Shearing and Stamping Company, Youngstown
56. Vorster TEB, Klar A, Soga K, Mair RJ (2005) Estimating the effects of tunneling on existing pipelines. J Geotech Geoenviron Eng 131(11):1399–1410
57. Yihdego Y (2017) Hydraulic in situ testing for mining and engineering design: packer test procedure, preparation, analysis and interpretation. Geotech Geol Eng 35(1):29–44. https://doi.org/10.1007/s10706-016-0112-9

58. Zou J, Chen G, Qian Z (2019) Tunnel face stability in cohesionfrictional soils considering the soil arching effect by improved failure models. Comput Geotech 106:1–17. https://doi.org/10.1016/j.compgeo.2018.10.014
59. Nazile, URAL Guncelleyiniz, GUNCELLEYİNİZ Evren, POŞLUK Discontinuity Controlled Deformation Estimation in small Diameter Tunnels El-Cezeri 9 (2): 829–842. https://doi.org/10.31202/ecjse.1013656
60. Das R, Singh PK, Kainthola A, Panthee S, Singh TN (2017) Numerical analysis of surface subsidence in asymmetric parallel highway tunnels. J Rock Mechan Geotechn Eng 9(1):170–179. https://doi.org/10.1016/j.jrmge.2016.11.009
61. Yan-jun S, Rui-xin Y, Geng-she Y, Guang-li X, Shan-yong W (2017) Comparisons of Evaluation Factors and Application Effects of the New [BQ]GSI System with International Rock Mass Classification Systems. Geotechn Geol Eng 35(6):2523–2548. https://doi.org/10.1007/s10706-017-0259-z
62. Kirsch EG (1898) The theory if elasticity and the need of the strength of materials (trans.). J Assoc German Eng 42:797–807

Publisher's Note